Charm sea effects on charmonium decay constants and heavy meson masses

THE EUROPEAN
PHYSICAL JOURNAL C

Regular Article - Theoretical Physics

Charm sea effects on charmonium decay constants and heavy meson masses

ALPHA Collaboration

Salvatore Calì[1,2,a]**, Kevin Eckert**[3]**, Jochen Heitger**[3]**, Francesco Knechtli**[4]**, Tomasz Korzec**[4]

[1] Center for Theoretical Physics, Massachusetts Institute of Technology, Cambridge, MA 02139, USA
[2] Institute of Theoretical Physics, Jagiellonian University, ul. Łojasiewicza 11, 30-348 Kraków, Poland
[3] Institut für Theoretische Physik, Westfälische Wilhelms-Universität Münster, Wilhelm-Klemm-Straße 9, 48149 Münster, Germany
[4] Department of Physics, Bergische Universität Wuppertal, Gaußstr. 20, 42119 Wuppertal, Germany

Abstract We estimate the effects on the decay constants of charmonium and on heavy meson masses due to the charm quark in the sea. Our goal is to understand whether for these quantities $N_f = 2 + 1$ lattice QCD simulations provide results that can be compared with experiments or whether $N_f = 2 + 1 + 1$ QCD including the charm quark in the sea needs to be simulated. We consider two theories, $N_f = 0$ QCD and QCD with $N_f = 2$ charm quarks in the sea. The charm sea effects (due to two charm quarks) are estimated comparing the results obtained in these two theories, after matching them and taking the continuum limit. The absence of light quarks allows us to simulate the $N_f = 2$ theory at lattice spacings down to 0.023 fm that are crucial for reliable continuum extrapolations. We find that sea charm quark effects are below 1% for the decay constants of charmonium. Our results show that decoupling of charm works well up to energies of about 500 MeV. We also compute the derivatives of the decay constants and meson masses with respect to the charm mass. For these quantities we again do not see a significant dynamical charm quark effect, albeit with a lower precision. For mesons made of a charm quark and a heavy antiquark, whose mass is twice that of the charm quark, sea effects are only about 1‰ in the ratio of vector to pseudoscalar masses.

Contents

1 Introduction

In recent years there has been a renewed interest in spectral calculations of charmonium states, which are bound systems made of a charm quark c and a charm antiquark $\bar{c}$. The motivation is due to the experimental discovery of many unexpected states, whose properties are still poorly understood [1]. Different hypotheses have been put forward, that see them identified as hybrid mesons, tetra-quarks or some other hitherto unknown form of matter. Other systems of particular interest are the B_c mesons, which are heavy mesons composed of a bottom quark (antiquark) and a charm antiquark (quark). Their peculiarities rely on the fact that they are the only heavy mesons consisting of heavy quarks with different flavors. Therefore, they cannot annihilate into gluons and they are more stable, having decay widths less than a hundred of keV. Only the pseudoscalar B_c has so far been seen at the Tevatron collider at Fermilab [2,3]. The high luminosity of the LHC collider at CERN now allows to measure the spec-

a e-mail: calis@mit.edu (corresponding author)

Springer

troscopy and the decay of $B_c^\star$ mesons with much better precision and therefore, comparisons of theoretical predictions with experiments will become more and more important.

Lattice QCD may represent a powerful tool to understand the properties of charmonium and B_c mesons directly starting from the QCD Lagrangian, for recent calculations see [4–7] (charmonium), [8] (charmonium decay constants) and [9] (B_c mesons). Depending on the problem at hand, numerical simulations usually include the lightest two, three or four flavors. Moreover, exact isospin symmetry is often assumed, implying that the lightest two quarks (up and down) are mass degenerate. The setups mentioned above are usually referred as $N_f = 2$, $N_f = 2 + 1$ and $N_f = 2 + 1 + 1$ QCD. Even though lattice QCD simulations with $N_f = 2 + 1 + 1$ dynamical quarks would be highly desirable to have a better understanding of physical phenomena governed by the strong interaction, the addition of a dynamical charm quark to the sea typically complicates the generations of the gauge configurations on which observables are computed. Also, if lattice spacings are not fine enough, the results may be affected by large cutoff effects, owing to the heavy mass of the charm quark.

Given the present difficulties described above, in this work we want to quantify how much quenching the charm quark affects the results obtained through $N_f = 2 + 1$ QCD simulations (including mass degenerate up, down and a strange quarks). To this aim, we consider a model of QCD, namely QCD with two degenerate heavy quarks, whose mass is tuned to approximately reproduce the physical value of the charm quark mass. In order to quantify the impact of the dynamical heavy quarks, the results from this model are then compared to the ones found using $N_f = 0$ QCD (all quarks are quenched). The advantage of our strategy is that reliable continuum extrapolations can be performed, because light quarks are absent and we can use gauge ensembles with extremely fine lattice spacings ($a \lesssim 0.02$ fm) and relatively small volumes. In Refs. [10–12] we followed this approach to evaluate the impact of a dynamical charm quark on the masses of charmonium states, e.g. on the pseudoscalar and vector meson masses m_P and m_V. From these studies it turned out that such effects are very small and for the hyperfine splitting $(m_V - m_P)/m_P$ they are of around 2%.

Here, we want to extend our previous studies and investigate the charm quark sea effects on the hyperfine splitting of heavy mesons H_c (bound states made of a heavy quark and a charm antiquark, or vice versa) and on the decay constants of charmonium. In particular, the focus is on the decay constants f_P and f_V of pseudoscalar and vector mesons, for which we follow the definitions of Ref. [13,14]

$$f_P m_P = \langle 0 | A_0^{q_1 q_2}(0) | P(\vec{p} = 0) \rangle, \tag{1.1}$$

$$f_V m_V = \frac{1}{3} \sum_{i=1}^{3} \langle 0 | V_i^{q_1 q_2}(0) | V_i(\vec{p} = 0) \rangle, \tag{1.2}$$

where the bilinears containing quarks q_1 and q_2 are

$$
\begin{aligned}
V_\mu^{q_1 q_2} &= \bar{q}_1 \gamma_\mu q_2, \\
A_\mu^{q_1 q_2} &= \bar{q}_1 \gamma_\mu \gamma_5 q_2, \\
P^{q_1 q_2} &= \bar{q}_1 \gamma_5 q_2,
\end{aligned}
\tag{1.3}
$$

and $|P\rangle$ and $|V_i\rangle$ represent the ground state of a pseudoscalar and vector meson polarized in the direction i of the vector current,[1] respectively. The meson spatial momentum is $\vec{p} = 0$ and $|0\rangle$ is the QCD vacuum state.[2] In the charmonium system, the lowest-lying states lie below the $D\bar{D}$ threshold, resulting in relatively narrow widths due to the absence of OZI allowed [16] strong decays. This means that radiative transitions, i.e. transitions from an initial state to a final state via the emission of a photon, can have significant experimentally accessible branching ratios. Therefore, the lattice calculation of the decay constants addressed here provides valuable theoretical insight for experiment on the fully non-perturbative level, such that we consider them as natural and representative observables to quantify charm sea quark effects in hadron physics beyond the mass spectrum.

The manuscript is organized as follows. In Sect. 2 we describe how decoupling works for observables which depend explicitly on the charm quark. In Sect. 3 we present our ensembles of gauge configurations with $N_f = 2$ charm quarks in the sea and $N_f = 0$ (pure gauge). The observables, from which we extract the decay constants and the heavy meson masses, are explained in Sect. 4, together with the tuning of the charm quark mass. The latter involves derivatives with respect to the heavy quark mass and we define suitable mass dependence functions in Sect. 4. Section 5 describes the distance preconditioning for the computation of the heavy quark propagator. The results of our calculations are presented in Sect. 6 and summarized in the conclusions (Sect. 7). Appendix A tabulates the values of the decay constants and their derivatives on our ensembles. Appendix B shows a derivation of the formula for the mass derivative in the effective theory which accounts for the dependence of the scale of the effective theory on the mass of the heavy quarks.

2 Decoupling in the presence of heavy valence quarks

The decoupling of heavy quarks from low-energy physics is well understood [17–20] and is known to work very well

---

[1] A definition of f_V with general vector meson polarization can be found in Eq. (12) of [15].

[2] Note that we are using the convention for which the pion decay constant takes the value $f_\pi = 130$ MeV.

already with heavy quarks as light as the charm quark [21–23]. QCD with light and a charm quark, described by the Euclidean action

$$S_I = S^{\text{YM}}[A_\mu] + S^{\text{light}}[\bar\psi_{u,d,s}, \psi_{u,d,s}, A_\mu]$$
$$+ (\bar\psi_c, [\slashed{D}[A_\mu] + m_c]\psi_c), \qquad (2.1)$$

where $(\ldots, \ldots)$ denotes the standard inner product for spinors, can be approximated by an effective theory, which to leading order is given by QCD without the heavy quarks

$$S_I^{\text{dec}} = S^{\text{YM}}[A_\mu] + S^{\text{light}}[\bar\psi_{u,d,s}, \psi_{u,d,s}, A_\mu]. \qquad (2.2)$$

When the couplings of the effective theory are correctly "matched", they inherit a dependence on the heavy quark mass of the fundamental theory, and the effective theory reproduces results of the fundamental one, as long as the observables do not contain heavy quarks and are low-energy quantities. The differences between the two theories are of order $O((\Lambda/\overline{m}_c)^2)$, $O((\overline{m}_{\text{light}}/\overline{m}_c)^2)$ and $O((E/\overline{m}_c)^2))$, where E is the energy scale associated with the observable at hand, e.g. a momentum transfer in a process involving the light quarks, and $\overline{m}_{c,\text{light}}$ are the running masses of light and charm quarks. These differences could in principle be suppressed further by adding additional terms to the effective action, e.g.

$$\frac{c}{m_c^2}(\bar\psi_{\text{u,d,s}}, \psi_{\text{u,d,s}})^2. \qquad (2.3)$$

It is common practice in lattice QCD, to simulate one of the effective theories instead of full QCD. In particular, b and t quarks are never included in the simulations while the c quark sometimes is included and sometimes not. Even without c quarks in the action, charm physics is studied in the "partially quenched" approximation. Before we study how well this approximation works numerically, we would like to argue that it is to some extent covered by the theory of decoupling, even though the observables now *do* depend on the charm quarks. We can add two terms to S_I that amount to a factor of 1 in the path integral

$$S_{II} = S_I + (\bar\psi_{c'}, [\slashed{D}[A_\mu] + m_c]\psi_{c'}) + (\phi_{c'}^\dagger, [\slashed{D}[A_\mu] + m_c]\phi_{c'}). \qquad (2.4)$$

While $\psi_{c'}$ is a Grassmann-valued fermion field, ϕ is a complex-valued "pseudo-fermion" field with the same space-time, color and spin components. After integration over the fermion and pseudo-fermion fields, the fermionic determinant is exactly cancelled by the determinant from the pseudo-fermion Gaussian integral.[3] Therefore, expectation values in

the two theories are equal

$$\langle \mathcal{O}[\bar\psi_{u,d,s}, \psi_{u,d,s}, \bar\psi_c, \psi_c, A_\mu] \rangle_I$$
$$= \langle \mathcal{O}[\bar\psi_{u,d,s}, \psi_{u,d,s}, \bar\psi_c, \psi_c, A_\mu] \rangle_{II}$$
$$= \langle \mathcal{O}[\bar\psi_{u,d,s}, \psi_{u,d,s}, \bar\psi_{c'}, \psi_{c'}, A_\mu] \rangle_{II}. \qquad (2.5)$$

The decoupling mechanism can now be applied to the ψ_c fields in S_{II}, leading to a leading-order effective theory

$$S_{II}^{\text{dec}} = S_I^{\text{dec}} + (\bar\psi_{c'}, [\slashed{D}[A_\mu] + m_c]\psi_{c'})$$
$$+ (\phi_{c'}^\dagger, [\slashed{D}[A_\mu] + m_c]\phi_{c'}). \qquad (2.6)$$

After matching of the parameters (gauge coupling, light quark masses and the mass of the "partially quenched" charm quark), one expects

$$\langle \mathcal{O}[\bar\psi_{u,d,s}, \psi_{u,d,s}, \bar\psi_{c'}, \psi_{c'}, A_\mu] \rangle_{II}$$
$$= \langle \mathcal{O}[\bar\psi_{u,d,s}, \psi_{u,d,s}, \bar\psi_{c'}, \psi_{c'}, A_\mu] \rangle_{II}^{\text{dec}} + O(1/m_c^2). (2.7)$$

With the mass of the c' quark being the same as the one that was integrated out, one can of course expect large $O(1)$ corrections, but in some cases the energy scale of the observable may still be low, even if it contains heavy quarks. For example, the binding energies in charmonia are not very high, compared to the charm quark mass. In the same respect, another case are their decay constants which turn out to be not very large.

3 Numerical setup

Our calculations are performed on the gauge ensembles with parameters summarized in Table 1.

The $N_{\text{f}} = 0$ ensembles are generated using the standard Wilson plaquette gauge action [25], whilst for the $N_{\text{f}} = 2$ case a clover-improved [26] doublet of twisted mass Wilson fermions [27,28] is added.

Since we aim at performing continuum extrapolations using very fine lattice spacings, open boundary conditions in the time direction are applied [29] to avoid the well known problems related to the deficient sampling of topological sectors. The spatial dimensions are kept periodic. Moreover, for the production of our ensembles we benefit from the knowledge of the critical mass m_{cr} [30,31] and the axial current and pseudoscalar density renormalization factors Z_A [32–34] and Z_P [30,35]. For further details about the simulations we refer to our previous works [12,22] and references therein.

---

[3] This argument can be made more rigorous on the lattice, e.g. with Wilson fermions, and depends on m_c being large enough for the Wilson operator to only have eigenvalues with positive real parts.

4 Observables

4.1 Computation of meson decay constants with open boundary conditions

Meson decay constants are related to matrix elements between the vacuum and the meson state at rest, as anticipated in Eqs. (1.1) and (1.2). In the framework of the model considered here, we denote the doublet of the heavy degenerate charm quarks in the physical basis as $\psi = (\tilde{c}_1, \tilde{c}_2)^\mathsf{T}$ and its counterpart in the twisted basis as $\chi = (c_1, c_2)^\mathsf{T}$. At maximal twist, the relation between physical and twisted basis is

$$\psi = \frac{1 + i\gamma_5\tau^3}{\sqrt{2}}\chi, \quad \bar{\psi} = \bar{\chi}\frac{1 + i\gamma_5\tau^3}{\sqrt{2}}. \tag{4.1}$$

Therefore, the decay constants of pseudoscalar (P) and vector (V) mesons in twisted mass QCD are given by

$$f_P m_P^2 = 2\mu \, \langle 0|\bar{c}_1\gamma_5 c_2|P\rangle, \tag{4.2}$$

$$f_V m_V = \frac{1}{3}\sum_{i=1}^{3}\langle 0|\bar{c}_1\gamma_i\gamma_5 c_2|V_i\rangle, \tag{4.3}$$

where μ is the twisted mass parameter. To derive Eq. (4.2), PCVC relations in the twisted basis have been used, as described in Refs. [36,37]. Since both our quarks, c_1 and c_2, have the mass of a charm quark, $f_{P,V}$ and $m_{P,V}$ are comparable to the decay constants and masses of the charmonia states η_c and J/ψ. The main differences are related to the fact that in our calculations we neglect the contribution of disconnected diagrams and we are assuming a model of QCD without light quarks and with two charm quarks instead of one.

The twisted mass formulation of QCD provides a particularly convenient setup for the calculation of the pseudoscalar decay constant f_P, because it simplifies the renormalization properties of our operators. In fact, the renormalization factors Z_P and Z_μ obey the relation $Z_P Z_\mu = 1$. Thus, the lattice calculation of f_P does not need any renormalization factors, as already discussed in Refs. [27,36]. As concerns the twisted mass expression for f_V, the matrix element in Eq. (4.3) must be multiplied by the renormalization factor Z_A of the axial current, which is known from Refs. [32–34] for the ensembles considered here.

To extract the decay constants f_P and f_V given in Eqs. (4.2) and (4.3), we first need to know the values of the masses m_P and m_V (already computed in Ref. [12]) and of the matrix elements $\langle 0|\bar{c}_1\gamma_5 c_2|P\rangle$ and $\langle 0|\bar{c}_1\gamma_i\gamma_5 c_2|V_i\rangle$. All these quantities can be determined from the lattice calculation of zero-momentum correlation functions of the form

$$a^3 f_{PP}(x_0, y_0) = -\frac{a^3}{L^3}$$
$$\times \sum_{\vec{x},\vec{y}} a^6 \langle P^{c_1 c_2}(x_0, \mathbf{x}) P^{c_2 c_1}(y_0, \mathbf{y})\rangle, \tag{4.4}$$

$$a^3 f_{A_i A_i}(x_0, y_0) = -\frac{a^3}{L^3}$$
$$\times \sum_{\vec{x},\vec{y}} a^6 \langle A_i^{c_1 c_2}(x_0, \mathbf{x}) A_i^{c_2 c_1}(y_0, \mathbf{y})\rangle, \tag{4.5}$$

where $(y_0, \mathbf{y})$ and $(x_0, \mathbf{x})$ denote the coordinates at which a particle state is created (source) and annihilated (sink), respectively. Integrating over the fermion fields, one obtains

$$a^8 \sum_{\vec{x},\vec{y}} \langle \bar{c}_1(x)\Gamma c_2(x)\bar{c}_2(y)\Gamma c_1(y)\rangle_F$$
$$= -\sum_{\vec{x},\vec{y}} \text{Tr}\left[\Gamma D_{c_2}^{-1}(x, y)\Gamma D_{c_1}^{-1}(y, x)\right], \tag{4.6}$$
$$\Gamma = \{\gamma_5, \gamma_i\gamma_5\},$$

where $\langle\ldots\rangle_F$ is the expectation value over the fermion fields and $D_{c_1}^{-1}$, $D_{c_2}^{-1}$ are the fermion propagators of the quark c_1 and c_2, respectively. The trace in Eq. (4.6) can be efficiently estimated stochastically. In particular, we use time-dilution with 16 $U(1)$ noise sources per time-slice, which amounts to 16 inversions per y_0 value and Dirac structure Γ. In principle, the projection to zero-momentum can be realized performing a sum either over $\vec{x}$ or $\vec{y}$. However, here we prefer to keep the two sums, as indicated in Eqs. (4.4) and (4.5), because that typically leads to highly improved signals for the meson correlators.

The pseudoscalar and vector meson masses are extracted from the exponential decay of the correlators (4.4) and (4.5), respectively. For this purpose, we first compute the effective mass

$$am^{eff}(x_0 + a/2, y_0) \equiv \ln\left(\frac{f(x_0, y_0)}{f(x_0 + a, y_0)}\right) \tag{4.7}$$

and then perform a weighted average in the plateau region as

$$am = \frac{\sum\limits_{x_0/a=t_i}^{t_f} w(x_0 + a/2, y_0)am_{eff}(x_0 + a/2, y_0)}{\sum\limits_{x_0/a=t_i}^{t_f} w(x_0 + a/2, y_0)}, \tag{4.8}$$

where $x_0/a = t_{i,f}$ are the initial and final time-slices of the plateau, chosen such that the results do not depend on source position y_0 and excited state contributions are sufficiently suppressed. The weights w are given by the inverse squared errors of the corresponding effective masses.

In principle, even the matrix elements $\langle 0|\bar{c}_1\gamma_5 c_2|P\rangle$ and $\langle 0|\bar{c}_1\gamma_i\gamma_5 c_2|V\rangle$ can be extracted through an exponential fit to the meson correlators (4.4) and (4.5). However, since we

use open boundary conditions in the time direction, such an approach may lead to unreliable results, because of boundary effects. For this reason, we proceed along the method described in Refs. [38,39], whose advantage is to remove the unwanted boundary effects by forming a suitable ratio of two-point correlation functions.

Following the procedure of Ref. [39], when x_0 is far enough from the boundaries ($0 \ll x_0 \ll T$) and $x_0 - y_0$ is sufficiently large, it is possible to show that the correlators f_{PP} and $f_{A_i A_i}$ have a leading asymptotic behavior according to[4]

$$\sqrt{2m_P L^3} f_{PP}(x_0, y_0) \simeq \langle 0|\bar{c}_1 \gamma_5 c_2|P\rangle e^{-m_P(x_0-y_0)} A(y_0), \tag{4.9}$$

$$\sqrt{2m_P L^3} f_{PP}(T - x_0, y_0)$$
$$\simeq \langle 0|\bar{c}_1 \gamma_5 c_2|P\rangle e^{-m_P(T-x_0-y_0)} A(y_0), \tag{4.10}$$

$$L^3 f_{PP}(T - y_0, y_0) \simeq e^{-m_P(T-2y_0)} A^2(y_0), \tag{4.11}$$

$$\sqrt{2m_V L^3} f_{A_i A_i}(x_0, y_0)$$
$$\simeq \langle 0|\bar{c}_1 \gamma_i \gamma_5 c_2|V_i\rangle e^{-m_V(x_0-y_0)} B(y_0), \tag{4.12}$$

$$\sqrt{2m_V L^3} f_{A_i A_i}(T - x_0, y_0)$$
$$\simeq \langle 0|\bar{c}_1 \gamma_i \gamma_5 c_2|V_i\rangle e^{-m_V(T-x_0-y_0)} B(y_0), \tag{4.13}$$

$$L^3 f_{A_i A_i}(T - y_0, y_0) \simeq e^{-m_V(T-2y_0)} B^2(y_0), \tag{4.14}$$

where A, B are dimensionless factors depending on the source position y_0 and related to the matrix elements between the vacuum and the boundary state. From the relations (4.9)–(4.14) one reads off that the relevant amplitudes can be determined through the following ratios of correlators

$$R_P(x_0, y_0) \equiv \sqrt{\frac{a^3|f_{PP}(x_0, y_0) f_{PP}(T - x_0, y_0)|}{f_{PP}(T - y_0, y_0)}}$$
$$= \frac{a^2 \langle 0|\bar{c}_1 \gamma_5 c_2|P\rangle}{\sqrt{2am_P}}, \tag{4.15}$$

$$R_{A_i}(x_0, y_0) \equiv \sqrt{\frac{a^3|f_{A_i A_i}(x_0, y_0) f_{A_i A_i}(T - x_0, y_0)|}{f_{A_i A_i}(T - y_0, y_0)}}$$
$$= \frac{a^2 \langle 0|\bar{c}_1 \gamma_i \gamma_5 c_2|V_i\rangle}{\sqrt{2am_V}}. \tag{4.16}$$

Employing such ratios, the matrix elements of operators close to the boundary drop out, so there are no restrictions in the choice of the source position y_0. Equations (4.15) and (4.16) are satisfied for a large range of sink positions $0 \ll x_0 \ll T$, where boundary effects and excited state contributions can be neglected. Thus, to improve the estimate of the matrix

Fig. 1 Effective quantity R_P, defined in (4.15), from which the decay constants are extracted. The results shown in the figure are obtained on the $N_f = 2$ ensemble W at $\beta = 6.0$. The horizontal error band indicates the plateau average $\bar{R}_P$ with its statistical uncertainty

elements, we take the plateau averages

$$\bar{R}_P \equiv \frac{1}{t_f - t_i + 1} \sum_{x_0/a=t_i}^{t_f} R_P(x_0, y_0),$$

$$\bar{R}_{A_i} \equiv \frac{1}{t_f - t_i + 1} \sum_{x_0/a=t_i}^{t_f} R_{A_i}(x_0, y_0), \tag{4.17}$$

where t_i and t_f are the start and the end of the plateau. In Fig. 1 we report the measurement of the effective quantity R_P in Eq. (4.15) obtained on the $N_f = 2$ ensemble W, with parameters reported in Table 1. As can be seen, the use of lattices with large temporal extent and very fine lattice spacings allows us to take the plateau average $\bar{R}_P$ for a large range of temporal slices. Similar conclusions also hold for the other ensembles and the ratios R_{A_i}.

Finally, combining the formulae above, the pseudoscalar and vector decay constants f_P and f_V in lattice units can be determined as

$$af_P = 2a\mu \bar{R}_P \sqrt{\frac{2}{(am_P)^3}}, \tag{4.18}$$

$$af_V = Z_A \left(\frac{1}{3}\sum_{i=1}^{3} \bar{R}_{A_i}\right)\sqrt{\frac{2}{am_V}}. \tag{4.19}$$

The crucial point is to obtain a reliable estimate of the correlators $f_{PP}(T - y_0, y_0)$ and $f_{A_i A_i}(T - y_0, y_0)$ in Eqs. (4.15) and (4.16), as when dealing with heavy quarks the relative precision of the solution of the Dirac equation deteriorates at large distances. A detailed discussion of this issue will be given in Sect. 5. To improve the quality of the signal, we average over forward and backward correlator. Therefore, we

---

[4] The usual relativistic normalization of states in a finite volume is used, i.e. $\langle 0|0\rangle = 1$, $\langle P|P\rangle = 2m_P L^3$ and $\langle V_i|V_i\rangle = 2m_V L^3$.

Table 1 Simulation parameters of our ensembles. The columns show the lattice sizes, the gauge coupling $\beta = 6/g_0^2$, the critical hopping parameter, the twisted mass parameter μ, the pseudoscalar mass in t_0 units, the hadronic scale t_0/a^2 defined in [24], the lattice spacing in fm from the scale t_0 [12] and the total statistics in molecular dynamics units.

For the $N_f = 0$ ensembles, we report the values of $\sqrt{t_0}m_P$ measured at three different valence quark masses $a\mu$. The temporal extent T is an odd multiple of a because open boundary conditions are applied in the temporal directions and the links pointing out of the lattice volume are absent

N_f	ID	$\frac{T}{a} \times \left(\frac{L}{a}\right)^3$	β	κ	$a\mu$	$\sqrt{t_0}m_P$	t_0/a^2	a [fm]	MDUs
2	E	95×24^3	5.300	0.135943	0.36151	1.79303(55)	1.23907(82)	0.104	8000
	N	119×32^3	5.500	0.136638	0.165997	1.8048(15)	4.4730(93)	0.054	8000
	P	119×32^3	5.700	0.136698	0.113200	1.7931(28)	9.105(35)	0.038	17184
	S	191×48^3	5.880	0.136509	0.087626	1.8130(29)	15.621(60)	0.029	23088
	W	191×48^3	6.000	0.136335	0.072557	1.8075(43)	22.39(12)	0.024	22400
0	qN	119×32^3	6.100	–	0.16	1.69807(67)	4.4329(38)	0.054	64000
					0.17	1.76547(70)			
					0.18	1.83195(72)			
	qP	119×32^3	6.340	–	0.11	1.6856(22)	9.037(30)	0.038	20080
					0.12	1.7848(24)			
					0.13	1.8824(25)			
	qW	191×48^3	6.672	–	0.07	1.6830(28)	21.925(83)	0.024	73920
					0.08	1.8399(30)			
					0.09	1.9934(33)			
	qX	191×64^3	6.900	–	0.056	1.7714(28)	39.41(14)	0.018	160200
					0.058	1.8137(29)			
					0.060	1.8558(30)			

consider the symmetrized correlators

$$\bar{f}_{PP}(x_0, y_0) = \frac{1}{2} \left[f_{PP}(x_0, y_0) \right.$$
$$\left. + f_{PP}(T - x_0, T - y_0) \right], \qquad (4.20)$$

$$\bar{f}_{A_i A_i}(x_0, y_0) = \frac{1}{2} \left[f_{A_i A_i}(x_0, y_0) \right.$$
$$\left. + f_{A_i A_i}(T - x_0, T - y_0) \right]. \qquad (4.21)$$

As it was demonstrated in Appendix A of Ref. [12], taking the average with the time-reflected correlators prohibits the mixing with states of opposite parity.[5]

4.2 Heavy mesons

To study the charm loop effects at even higher energies, we measure the masses of heavy mesons H_c made of a heavy quark, h, with mass $m_h = \{m_c, 2m_c\}$. In particular, we focus on the ground state of the pseudoscalar and vector channels. The masses are extracted according to Eqs. (4.7), (4.8). The main ingredient of the calculation is the propagator D_h^{-1}, which is evaluated using the twisted mass parameter $\mu_h = \mu$ or $\mu_h = 2\mu$, depending on the value of the mass m_h we want

to impose. Let us recall that μ is the twisted mass parameter of the simulations tuned to reproduce the charm quark mass.

From now on, we refer to the masses of these heavy mesons using the notation

$$m_{X, H_c}, \quad X = \{P, V\}, \qquad (4.22)$$

where X denotes the vector or pseudoscalar state and the heavy quark, h, can have a mass equal to m_c or $2m_c$. The masses are extracted through the plateau average (4.8) of the effective mass (4.7). For the $m_h = m_c$ case, we refer to our previous work [12]. An example of this procedure for $m_h = 2m_c$ is shown in Fig. 2 for the $N_f = 2$ ensemble W.

4.3 Tuning of the twisted mass parameter

To match $N_f = 0$ and $N_f = 2$ QCD, we use the low-energy observable $m^{had} = 1/\sqrt{t_0}$. For such observables decoupling applies [17,40] and we can assume $\sqrt{t_0}|_{N_f=0} = \sqrt{t_0(M_c)}|_{N_f=2}$. In order to compare the two theories, the value of the renormalization group invariant (RGI) mass M_c of the charm quark needs to be fixed and, following the procedure of our previous work [12], we choose M_c such that $\sqrt{t_0}m_P$ is approximately equal to the physical value for the η_c meson and is the same in $N_f = 0$ and $N_f = 2$ QCD, for each lattice spacing employed (see Table 1).

---

[5] Parity is not a symmetry in the twisted mass formulation of QCD for twisted mass parameter $\mu \neq 0$.
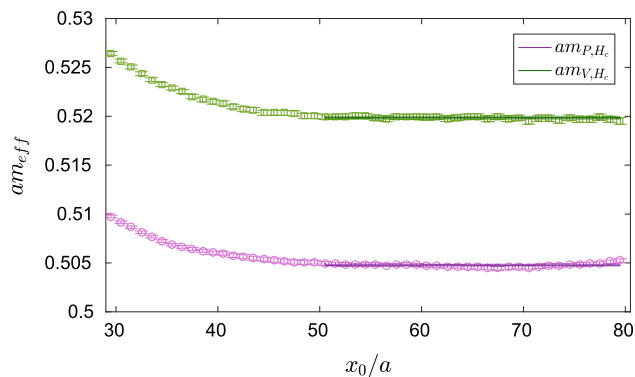
Fig. 2 The effective masses for heavy mesons made of a heavy quark h $(m_h = 2m_c)$ and a charm quark c on the W ensemble are displayed, together with the plateau average and its error band. We show the pseudoscalar (violet circles) and vector (green squares) channels

To set M_c we proceed as described below. On our finest $N_f = 2$ lattice ($\beta = 6.0$), the RGI mass M_c of the charm quark is fixed by the relation

$$M_c/\Lambda_{\overline{\text{MS}}} = 4.87, \tag{4.23}$$

where we use the value $M_c = 1510$ MeV of Ref. [41] (which agrees with Ref. [42], see also Ref. [43]) and the two-flavor Lambda parameter $\Lambda_{\overline{\text{MS}}} = 310(20)$ MeV known from [30]. Since on our $N_f = 2$ ensembles the hopping parameter κ is set to its critical value, the renormalized physical quark mass is simply given by $m_R = Z_P^{-1}\mu$ and the condition (4.23) is equivalent to fix the twisted mass parameter through

$$a\mu = \frac{M_c}{\Lambda_{\overline{\text{MS}}}} \times Z_P(L_1^{-1}) \times \frac{m_R(L_1)}{M_c} \times \Lambda_{\overline{\text{MS}}}L_1 \times \frac{a}{L_1}. \tag{4.24}$$

In the equation above, the value of the pseudoscalar renormalization factor Z_P at the renormalization scale L_1^{-1} in the Schrödinger Functional scheme

$$Z_P(L_1) = 0.5184(33), \quad \text{valid for } 5.2 \le \beta \le 6, \tag{4.25}$$

and the relation between the running mass $m_R(L_1)$ and the RGI mass

$$\frac{M}{m_R(L_1)} = 1.308(16) \tag{4.26}$$

are available from Refs. [30,44]. As a value of the Λ parameter of the two-flavor theory in L_1 units we take [45]

$$\Lambda_{\overline{\text{MS}}}L_1 = 0.649(45), \tag{4.27}$$

whilst the ratio L_1/a is known from [21]. Plugging the values of Eqs. (4.25)–(4.27) into Eq. (4.24), the charm quark mass can be fixed at a precision of around 10%. Such accuracy is acceptable for us if we devise a method to keep the relative mass differences between the different ensembles under better control. In practice, instead of using Eq. (4.24), we tune the twisted mass parameter to a point $\mu^\star$ such that the renormalized quantity $\sqrt{t_0}m_{\eta_c}$ is equal to its value on our finest

$N_f = 2$ ensemble W at $\beta = 6.0$ (see Table 1) and satisfies

$$\sqrt{t_0}m_P(\mu^\star) \equiv 1.807463. \tag{4.28}$$

This value is obtained on the ensemble W by setting the twisted mass parameter through Eq. (4.24). The tuning point Eq. (4.28) is independent of the overall scale $\Lambda_{\overline{\text{MS}}}$ (known with a 7% accuracy and which limits the overall accuracy).

In the $N_f = 2$ theory, we apply a correction to all observables, which is based on the computation of twisted mass derivatives [12]. First, we determine the target tuning point $\mu^\star$ through the Taylor expansion

$$\mu^\star = \mu + (\sqrt{t_0}m_P - 1.807463)\left(\frac{d\sqrt{t_0}m_{\eta_c}}{d\mu}\right)^{-1}, \tag{4.29}$$

where μ and $\sqrt{t_0}m_P$ are the values from the simulations obtained using Eq. (4.24), see Table 1. Subsequently all quantities, denoted by A below, are corrected by

$$A(\mu^\star) = A(\mu) + (\mu^\star - \mu)\frac{dA}{d\mu}. \tag{4.30}$$

For a generic primary observable A, its twisted mass derivative is simply given by

$$\frac{d\langle A\rangle}{d\mu} = -\left\langle\frac{dS}{d\mu}A\right\rangle + \left\langle\frac{dS}{d\mu}\right\rangle\langle A\rangle + \left\langle\frac{dA}{d\mu}\right\rangle, \tag{4.31}$$

where S is the lattice QCD action. However, most quantities we are interested in are non-linear functions f of various primary observables, for which we apply the chain rule

$$\frac{df(\langle A_1\rangle,\ldots,\langle A_N\rangle,\mu)}{d\mu} = \frac{\partial f}{\partial\mu} + \sum_{i=1}^{N}\frac{\partial f}{\partial\langle A_i\rangle}\frac{d\langle A_i\rangle}{d\mu}. \tag{4.32}$$

After integrating over the fermion fields, Eq. (4.31) becomes

$$\frac{d\langle\tilde{A}\rangle^{\text{gauge}}}{d\mu} = -\left\langle\frac{dS_{\text{eff}}}{d\mu}\tilde{A}\right\rangle^{\text{gauge}}$$
$$+ \left\langle\frac{dS_{\text{eff}}}{d\mu}\right\rangle^{\text{gauge}}\langle\tilde{A}\rangle^{\text{gauge}} + \left\langle\frac{d\tilde{A}}{d\mu}\right\rangle^{\text{gauge}}, \tag{4.33}$$

where $\langle\cdot\rangle^{\text{gauge}}$ are expectation values taken on the ensemble of gauge fields and S_{eff} is the effective lattice QCD gauge action which includes the effect of the fermion determinants. The observable $\tilde{A}$ contains in general the fermion propagator D^{-1}. The sea quark effects originate from $\frac{dS_{\text{eff}}}{d\mu}$. They affect the mass derivative of an observable through the covariance of $\frac{dS_{\text{eff}}}{d\mu}$ and $\tilde{A}$.

In the simplest case of $N_f = 0$ QCD, the action does not depend on the quark masses and the twisted mass parameter μ only enters the inversions of the Dirac operator. The mass derivative of an observable in the $N_f = 0$ theory therefore only receives a contribution from the last term on the right hand side of Eq. (4.33). Thus, to reproduce the tuning point $\mu^\star$, Eq. (4.28), for our $N_f = 0$ ensembles, we measure the quantities of interest at three different values of the twisted

mass parameter μ such that $\mu^\star$ is eventually obtained through a linear interpolation of the measurements.

4.4 Mass dependence functions

The mass dependence of a multiplicatively renormalizable quantity X is captured by the renormalized combination

$$\eta_X \equiv \frac{M}{X} \frac{dX}{dM}. \tag{4.34}$$

Interesting quantities X are for instance the vector or pseudoscalar meson masses as studied in [12], or their decay constants, as determined in this work. In the twisted mass formulation at maximal twist, the RGI quark mass is connected multiplicatively to the twisted mass parameter μ, which implies that M can be replaced by μ in Eq. (4.34). When computed in the effective theory, the mass dependence stems from an explicit mass dependence of the quantity in question, but also from the mass dependence that the scale inherits through the matching condition between the effective and full theory. In this context it is useful to also define

$$\tilde{\eta}_X \equiv \frac{M}{X} \frac{dX}{dM}\bigg|_{\Lambda=\text{const.}}. \tag{4.35}$$

In the fundamental theory, Λ is constant and $\tilde{\eta}_X = \eta_X$, but in the effective theory $\tilde{\eta}_X$ captures only the explicit mass dependence of the quantity in question and vanishes e.g. for purely gluonic quantities. It has been computed in [12] for the masses[6] and found to deviate significantly from the corresponding two-flavor values. Most of this deviation is explained by the neglected mass dependence associated with the scale. If the mass parameter in the $N_\text{f} = 0$ theory is fixed by demanding that m_P has the same value as in the $N_\text{f} = 2$ theory, the full mass dependence is given by

$$\eta_X^{(0)} = \eta^M + \frac{\tilde{\eta}_X^{(0)}}{\tilde{\eta}_{m_P}^{(0)}} \left(\eta_{m_P}^{(2)} - \eta^M \right) + O(M^{-2}). \tag{4.36}$$

In this equation, η^M denotes the universal mass scaling function introduced in [46], which encodes the complete mass dependence of purely gluonic quantities. Its definition is

$$\eta^M = \frac{M}{P_{2,0}} \frac{\partial P_{2,0}}{\partial M}\bigg|_{\Lambda^{(2)}}, \tag{4.37}$$

where $P_{2,0}$ is defined in Eq. (B.3) and $M \equiv M^{(2)}$. A derivation of Eq. (4.36) is relegated to Appendix B.

---

[6] The quantities $\eta_{P,V}$ in [12] for $N_\text{f} = 2$ correspond to η_{m_P,m_V} here, and for $N_\text{f} = 0$ correspond to $\tilde{\eta}_{m_P,m_V}$.

5 Distance preconditioning for the Dirac operator

The computation of R_P and R_{A_i} in Eqs. (4.15) and (4.16) requires the evaluation of the two-point correlation functions $\bar{f}_{PP}(T-y_0, y_0)$ and $\bar{f}_{A_i A_i}(T-y_0, y_0)$. These are constructed in the standard way in terms of quark propagators that result from solving the Dirac equation $\sum_x D(y, x)\psi(x) = \eta(y)$, where $D(y, x)$ is the lattice Dirac operator, while $\psi(x)$ and $\eta(y)$ denote the solution vector and the source field (the latter being non-zero only on a single time-slice y_0), respectively. Whereas the increase of computational demand for the numerical inversion of the Dirac operator to solve this linear system towards small quark masses is a consequence of the spectral properties of $D(x, y)$, a difficulty of entirely different nature arises in the region of heavy quark masses.

To understand the origin of this potentially serious problem, we recall that the exponential decay with time of two-point functions at zero spatial momentum is governed by the ground state energy in its spectral decomposition, which equivalently reflects in the exponential time dependence of the entering quark propagators proportional to $\exp\{-m_q(x_0 - y_0)\}$, where m_q is the quark mass in the corresponding Dirac operator. However, the exponential decay of the quark propagator is particularly pronounced in the case of heavy quarks, $m_q = m_h$, when the time distance between source and sink grows. This entails that an accurate determination of heavy meson correlators over the relevant time span is very difficult to achieve, because, depending on the size of the heavy quark mass in lattice units, the relative precision of the solution of the Dirac equation could actually start to deteriorate at already moderately large time separations $x_0 - y_0$. Moreover, this problem is amplified for correlation functions in the vector channel, in which the ground state is even heavier.

In practice, for heavy quarks, the stopping criterion commonly imposed on the relative *global residuum*

$$\frac{\left| \sum_y [D\psi(y) - \eta(y)] \right|}{\left| \sum_y \eta(y) \right|} < r_\text{gl} \tag{5.1}$$

may therefore no longer appear as a reliable quantitative measure to indicate the convergence of the iterative routine used to numerically solve the Dirac equation to desired accuracy. In fact, for large time separations $x_0 - y_0$, contributions to the norm on the l.h.s. suffer from a severe exponential suppression $\propto \exp\{-m_h(x_0 - y_0)\}$ and thus become negligible. Even a "brute force" approach of reducing the global residual r_gl further to catch this may then not be feasible anymore for lattices with very large time extents, regardless of the related increase in computational cost.

To overcome this unwanted exponential suppression problem induced by the heavy quark propagator, we employ the

distance preconditioning (DP) technique for the Dirac operator, originally proposed in Ref. [47], in its implementation outlined in [48]. The basic idea is to rewrite the original linear system in such a way that the solution of the new system at time-slices x_0 far away from the source gets exponentially enhanced and thereby compensates the rapid decay of the (heavy) quark propagator. While in [47] the associated redefinition of the propagator and source field was introduced on the level of the covariant derivatives in the lattice Dirac operator, the DP implementation of Ref. [48] directly works with the matrix-vector equation to be solved, since this has proven to be most straightforward for, e.g., the SAP-GCR solver routine [49] in use. Schematically written, DP then amounts to replace

$$D\psi = \eta \quad \rightarrow \quad D'\psi' = \eta',$$
$$D' = MDM^{-1}, \quad \psi' = M\psi, \quad \eta' = M\eta, \qquad (5.2)$$

where in our setup the preconditioning matrix is defined as

$$M = M(x_0 - y_0) = \text{diag}\left(p_0, p_1, \ldots, p_{T/a}\right) \quad \text{with}$$
$$p_i = \exp\left\{\alpha_0\left(x_0^{(i)} - y_0\right)\right\}. \qquad (5.3)$$

Here, y_0 and $x_0^{(i)}$ refer to the time-slices of the source and sink insertion, and apart from this, M is unity in spatial coordinates as well as in spin and color spaces. The solution of the original system is then simply obtained by $\psi = M^{-1}\psi'$ from the solution of the preconditioned one. In Eq. (5.3), α_0 is a tunable parameter that needs to be adjusted for each gauge field configuration ensemble in dependence of the respective temporal lattice extent and heavy quark mass in lattice units.

Rather than the global residual, Eq. (5.1), a more suitable measure for the numerical quality of the solution over the whole time range is now provided by inspecting the *local residuum*,

$$r_{\text{loc}}(x_0 - y_0) = \frac{\left|\sum_{\vec{y}}[D\psi(y) - \eta(y)]\right|}{\left|\sum_{\vec{y}}\psi(y)\right|}, \qquad (5.4)$$

at the time separation of interest ($T - 2y_0$ in our case). Since r_{loc} is sensitive to the numerical accuracy of the solution on each time-slice, imposing the stopping criterion of the routine involved to solve the preconditioned system ensures to extract heavy meson correlation functions to sufficient precision also for large time separations. Note that the exponential factor $e^{\alpha_0(x_0-y_0)}$ in the construction of the preconditioned linear system, Eq. (5.2) above, effectively turns the heavy quark propagator into a propagator corresponding to a "ficticious" light quark. Therefore, the price to pay when adopting this method is an increase of the number of solver iterations such that in practical applications the growth in computational

costs has to be reasonably balanced with the gain in accuracy of the heavy meson correlator in question by a proper tuning of α_0.

As can be seen from monitoring r_{loc} for a representative ensemble and various choices of α_0 in Fig. 3, the solution becomes more and more accurate as α_0 increases. However, in this example we observe that for the solution to have a local residual $< 10^{-4}$ for all time-slices (which is enough given the desired statistical accuracy of the meson correlator) the number of solver iterations increases of around a factor 3 compared to the case $\alpha_0 = 0$ (no distance preconditioning applied).

Such a small value of the residual is crucial to extract the meson correlator (and as a consequence the meson decay constants) reliably. Ideally one would choose $y_0 = a$, but to keep the computational effort as small as possible, we explored different source positions (with $y_0 > a$) to ensure the ground state dominance over a large range of time-slices and a reasonable number of iterations for the solver to converge.

Both R_P and R_{A_i} have been determined for all the ensembles under study and the parameters used in the solver setup are collected in Table 2.

6 Results

6.1 Decay constants of charmonium

Combining the measurements of the ratios R_P and R_{A_i}, defined in Eqs. (4.15) and (4.16), with the charmonium masses that we previously obtained in Ref. [12], through Eqs. (4.18) and (4.19), we determine the dimensionless quantities $\sqrt{t_0}f_P$ and $\sqrt{t_0}f_V$. They are listed in Appendix A.

Similarly to what we observed for the meson masses in Ref. [12], we find that linear fits in a^2 do not work well in the range of lattice spacings $0.02\,\text{fm} \lesssim a \lesssim 0.07\,\text{fm}$, if one aims at results with sub-percent precision. Therefore, we compare the continuum limits of pseudoscalar and vector decay constants in $N_{\text{f}} = 0$ and $N_{\text{f}} = 2$ QCD, performing extrapolations to zero lattice spacing only in the range $0.02\,\text{fm} \lesssim a \lesssim 0.05\,\text{fm}$. The results for the $N_{\text{f}} = 0$ (empty markers) and $N_{\text{f}} = 2$ (full markers) ensembles are shown in Fig. 4. The continuum limit values are slightly displaced for clarity.

Comparing the values obtained in the continuum of the two theories, one can observe that dynamical charm effects on the decay constants are barely resolvable, despite the great accuracy of our continuum extrapolations. In Table 3 we summarize our findings. The relative difference of $\sqrt{t_0}f_P$ is $([\sqrt{t_0}f_P]^{N_{\text{f}}=2} - [\sqrt{t_0}f_P]^{N_{\text{f}}=0})/[\sqrt{t_0}f_P]^{N_{\text{f}}=2} = 0.48(34)\%$, which corresponds to an effect of around 1.4σ.

Fig. 3 Tuning of the parameter α_0 of the distance preconditioning method for our coarsest lattice ($N_f = 2$, $\beta = 5.3$, see Table 1). We show the relative local residual of the solution ψ as a function of the sink position x_0 with respect to the source set at $y_0/a = 16$. On the right, the number of iterations for the solver to converge is reported for the values of α_0 plotted in the Figure

α_0	Iterations
0.00	265
0.10	287
0.20	335
0.30	411
0.40	536
0.50	768
0.60	1296
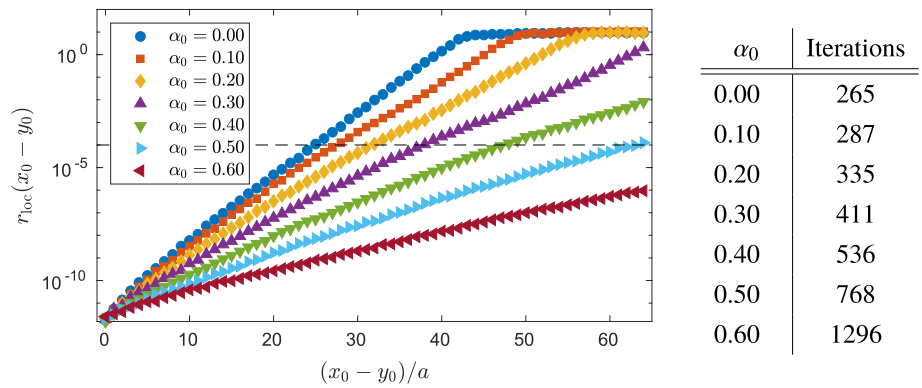
Table 2 The table lists the values of the parameter α_0 for the distance preconditioning of the Dirac operator and the time-slice of the source position used to determine R_P and R_{A_i}. Distance preconditioning is not used for the ensemble qX

Ensemble	α_0	y_0/a
E	0.40	24
N	0.10	30
P	0.05	20
S	0.01	48
W	0.02	32
qN	0.10	30
qP	0.05	20
qW	0.02	32
qX	0.00	32

Table 3 Results for $\sqrt{t_0} f_P$ and $\sqrt{t_0} f_V$ in the continuum limit for both the $N_f = 2$ and the $N_f = 0$ theory

Quantity	$N_f = 2$	$N_f = 0$	Sea effects [%]
$\sqrt{t_0} f_P$	0.25604(65)	0.25481(59)	0.48(34)
$\sqrt{t_0} f_V$	0.2806(17)	0.2810(13)	0.12(77)

Moreover, employing $\sqrt{t_0} = 0.1131(38)$ fm [21] for our model of QCD, we obtain[7]

$$f_P = 445.9(1.1) \text{ MeV},$$
$$f_V = 488.7(3.0) \text{ MeV} \qquad (N_f = 2), \qquad (6.1)$$
$$f_P = 443.8(1.0) \text{ MeV},$$
$$f_V = 489.4(2.2) \text{ MeV} \qquad (N_f = 0). \qquad (6.2)$$

Note that the decay constant of the meson η_c has not been determined experimentally, whilst for the vector meson J/ψ the value $f_{J/\psi} = 407(4)$ MeV is obtained from the partial decay width of J/ψ into an electron-positron pair, see [8]. $f_{J/\psi}$ can be compared to our lattice results for f_V in Eqs. (6.1) and (6.2). The discrepancy is probably due to effects of light sea quarks, disconnected contributions and electromagnetism, which are neglected in this work, and also to the unphysical values of the meson masses.

The mass dependence functions for meson masses and decay constants have been computed as well. Figure 5 shows how $\eta_X^{(2)}$ compares to both $\eta_X^{(0)}$ and $\tilde{\eta}_X^{(0)}$ for various quantities. In $\eta_X^{(2)}$ and $\tilde{\eta}_X^{(0)}$, the derivatives are computed using Eqs. (4.32) and (4.31). The missing pieces to evaluate Eq. (4.36) are the continuum value $\eta_{m_P}^{(2)} = 0.6996(81)$ from [12], and the value $\eta^M(M_c) = 0.1276(2)$ determined as in [21] for the $N_f = 2 \rightarrow N_f = 0$ case, using four- and five-loop perturbation theory results for the decoupling relations [19,20], the QCD β-function and the QCD anomalous dimension [50–54]. Table 4 summarizes the findings on
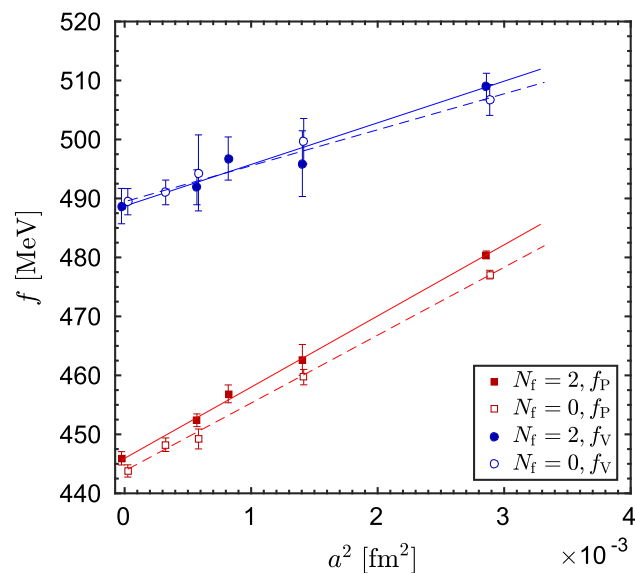
Fig. 4 Continuum extrapolations of the meson decay constants f_P and f_V on our $N_f = 2$ (full markers) and $N_f = 0$ (empty markers) ensembles. The continuum limit values are slightly displaced horizontally. To set the scale in physical units, we use $\sqrt{t_0} = 0.1131(38)$ fm [21]

---
[7] The $N_f = 2$ result (6.1) is obtained in QCD with two dynamical charm quarks but no light quarks. The $N_f = 0$ result (6.2) relies on decoupling to set the scale through the value of t_0 determined in the $N_f = 2$ theory.
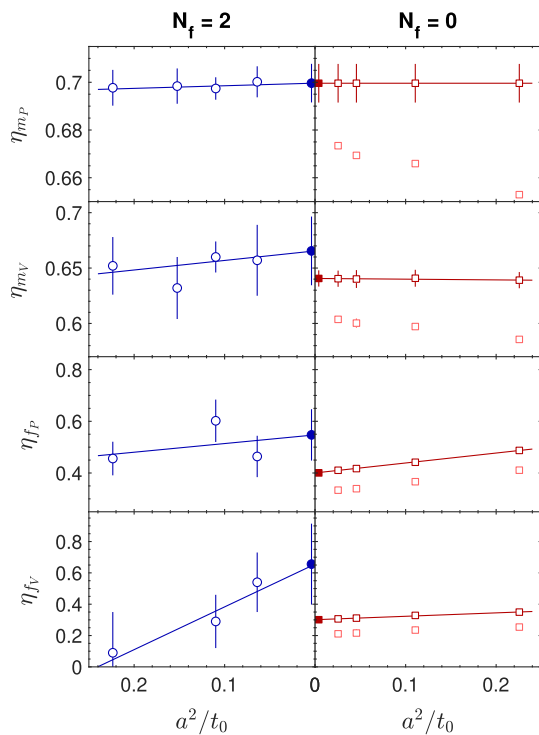
Fig. 5 Logarithmic derivative of the pseudoscalar and vector masses and decay constants with respect to the quark mass. Comparison between $N_f = 2$ and $N_f = 0$ theories. For the $N_f = 0$ case, the values of $\tilde{\eta}_X$, where the mass dependence of the scale is neglected, are shown in pink. When the scale dependence is taken into account, the errors increase due to a dependence on $\eta_{m_P}^{(2)}$

the mass dependence. Note that agreement is only observed when the mass dependence is consistently taken into account.

The charm sea quarks effects in the mass derivatives of an observable originate from the covariance of the mass derivative of the effective action with the observables, see Eq. (4.33). This covariance is absent in the $N_f = 0$ theory and explains the much larger statistical errors of the $N_f = 2$ theory. The derivatives computed on each ensemble are used to shift the decay constants to the tuning point, see Eq. (4.30). Still, they are physical quantities on their own.

6.2 Heavy meson masses

In this section we present our results for heavy mesons made up of a heavy quark h ($M_h = 2M_c$) and a charm quark c, as
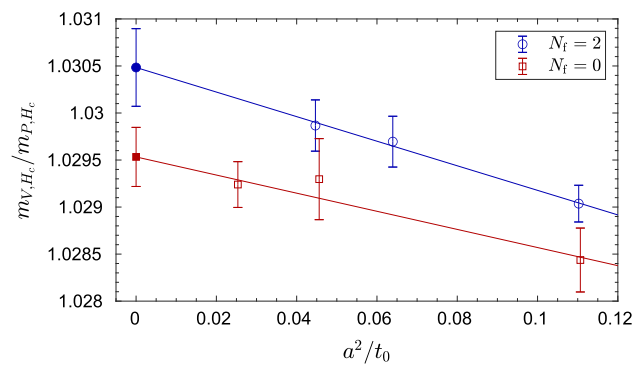
Fig. 6 Continuum limits of the ratio $m_{V,H_c}/m_{P,H_c}$ for $N_f = 2$ (blue circles) and $N_f = 0$ (red squares) QCD. The mass of the heavy quark is $M_h = 2M_c$

described in Sect. 4.2. To guarantee that the cutoff effects in the continuum extrapolations are under control, we only consider the ensembles of Table 1 for which the meson masses satisfy the relation $am < 1$.

In Fig. 6 we compare the continuum limits of the mass ratio $m_{V,H_c}/m_{P,H_c}$ in $N_f = 0$ and $N_f = 2$ QCD. The numerical results of the continuum extrapolations are summarized in the first row of Table 5. As it can be seen, the effect of dynamical charm quarks on the ratio $m_{V,H_c}/m_{P,H_c}$ is found to be 0.092(50)% (around 1.8σ), which is of similar size to the one obtained in our previous work [12] for $M_h = M_c$.

In Fig. 7 we show the hyperfine splitting $(m_{V,H_c} - m_{P,H_c})/\Lambda_{\overline{MS}}$ as a function of $\Lambda_{\overline{MS}}/M_h$, where M_h is the RGI mass of the heavy quark h. The blue circles correspond to the $N_f = 2$ theory and the red squares to the pure gauge theory, $N_f = 0$. We take the Λ parameters in units of the scale $\sqrt{t_0}$ [24] from [21,30] for $N_f = 2$ QCD and from [55] for $N_f = 0$ QCD. The RGI quark mass values $M_h = M_c$ at our tuning point Eq. (4.28) have been determined in [12] for both theories. The data of Fig. 7 are listed in Table 6.

The limit $M_h \to \infty$ is expected to be described by heavy quark effective theory (HQET). For $N_f = 0$ QCD we show in Fig. 7 a linear function (dashed line) going through the points at $M_h = \infty$, where the vector and the pseudoscalar are degenerate by virtue of the heavy quarks spin symmetry [56–58], and $M_h = 2M_c$. Contact with HQET in the spirit of [59], including the HQET-QCD matching factor C_{spin} that

Table 4 The mass dependence functions for various quantities in the continuum limit, at the charm quark mass. The results for the meson masses rely on data published in [12]. Note that in the first row $\eta_{m_P}^{(2)} = \eta_{m_P}^{(0)}$ because of the matching condition (B.2)

X	$\eta_X^{(2)}$	$\eta_X^{(0)}$	$\tilde{\eta}_X^{(0)}$
m_P	0.6996(81)	0.6996(81)	0.67553(42)
m_V	0.665(31)	0.6406(73)	0.6060(13)
f_P	0.547(99)	0.4003(43)	0.3233(19)
f_V	0.66(26)	0.3010(74)	0.2058(81)

Table 5 Results for $m_{V,H_c}/m_{P,H_c}$ in the continuum limit for both the $N_f = 0$ and the $N_f = 2$ theory. The values for the $M_h = M_c$ case are taken from Ref. [12]

Quantity	$N_f = 2$	$N_f = 0$	Sea effects [%]
$m_{V,H_c}/m_{P,H_c}$, $M_h = 2M_c$	1.03048(41)	1.02953(31)	0.092(50)
$m_{V,H_c}/m_{P,H_c}$, $M_h = M_c$	1.05405(60)	1.05274(46)	0.124(71)
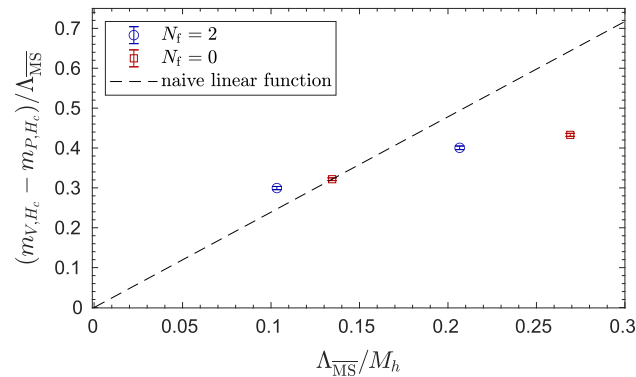
Fig. 7 The hyperfine splitting of heavy-charm mesons as a function of the inverse RGI heavy quark mass for $N_f = 2$ (blue circles) and $N_f = 0$ (red squares) QCD. The dashed line is a linear function which passes through the $N_f = 0$ points at infinite quark mass and $M_h = 2M_c$, and it has been extended to smaller quark masses

accounts for the correct mass dependence of the $M_h \to \infty$ asymptotics, would require larger heavy quark masses than we have simulated in this work.

7 Conclusions

In this work we present a study of the effects of sea charm quarks in the charmonium decay constants. It is a follow-up of Ref. [12] where we did a similar study for the charmonium spectrum and the RGI charm quark mass. We compute the charm-quark sea effects through a comparison of the decay constants determined in a model of QCD with only $N_f = 2$ charm quarks and no light quarks with those computed in the Yang–Mills theory ($N_f = 0$ QCD). The charm quark mass is fixed in both theories by the tuning condition Eq. (4.28), which approximately corresponds to a physical charm quark.

We find that the effects of two charm sea quarks are below 1% for the decay constant of the pseudoscalar (η_c) and of the

vector (J/ψ) ground state particles. We also extracted the derivatives of the decay constants and meson masses with respect to the charm quark mass, because they are required to shift our simulation results to the tuning point Eq. (4.28). The quantities $\eta_X = \frac{M}{X} \frac{dX}{dM}$ ($X = m_P, m_V, f_P, f_V$) are renormalized and easily computable in the twisted mass formulation at maximal twist, because the twisted mass parameter μ is multiplicatively renormalizable. In the continuum limit we do not see significant effects of the dynamical charm quark on these quantities.

A computation of the charm sea effects for "B_c" mesons made of a charm quark and an antiquark of twice larger mass reveals that they are only about 1‰ for the ratio of the vector to the pseudoscalar mass.

Our results are relevant for the scale setting [38] of the $N_f = 2 + 1$ simulations by the CLS consortium [60,61]. There, a combination of the pseudoscalar decay constants of the pion and kaon is used. They are lower in energy than the decay constants of charmonium. Hence our results indicate that charm sea effects are below the precision of the scale determination in [38]. Finally, the analysis of the "B_c" mesons also demonstrates that charm sea effects are very small for splittings of heavy mesons. For instance, the $\Upsilon - \Upsilon'$ splitting has been used in [62] for scale setting.

Table 6 Hyperfine splitting of heavy-charm mesons $(m_{V,H_c} - m_{P,H_c})/\Lambda_{\overline{MS}}$ as a function of Λ/M_h, where M_h is the RGI mass of the heavy quark h

M_h	$N_f = 2$		$N_f = 0$	
	$\Lambda_{\overline{MS}}/M_h$	$(m_{V,H_c} - m_{P,H_c})/\Lambda_{\overline{MS}}$	$\Lambda_{\overline{MS}}/M_h$	$(m_{V,H_c} - m_{P,H_c})/\Lambda_{\overline{MS}}$
$2M_c$	0.1033	0.2995(40)	0.1346	0.3217(34)
M_c	0.2066	0.4005(45)	0.2691	0.4330(38)

Table 7 Meson decay constants in t_0 units. For $N_f = 2$ simulations, the first line contains the values extrapolated to the tuning point $\mu^\star$ and the second line the values at the simulated parameters. For $N_f = 0$ ensembles, the first line gives the values interpolated to $\mu^\star$, and the following three lines contain the values measured at different valence quark masses. The last two columns are the values of the logarithmic derivatives of the decay constants with respect to the logarithm of the quark mass. For the ensemble W they have not been computed

Ensemble	$a\mu$	$\sqrt{t_0}f_P$	$\sqrt{t_0}f_V$	$\frac{\mu}{f_P}\frac{df_P}{d\mu}$	$\frac{\mu}{f_V}\frac{df_V}{d\mu}$
N	0.16647(28)	0.27582(38)	0.2922(13)		
	0.166	0.27553(41)	0.2923(13)	0.456(65)	0.09(26)
P	0.11482(32)	0.2656(15)	0.2847(32)		
	0.1132	0.2637(16)	0.2840(36)	0.602(82)	0.29(17)
S	0.08717(25)	0.26229(87)	0.2852(21)		
	0.087626	0.26291(84)	0.2860(18)	0.464(80)	0.54(19)
W	0.072557	0.25972(62)	0.2824(17)	–	–
qN	0.17632(11)	0.27390(42)	0.2909(15)	0.4109(18)	0.254(15)
	0.16	0.26314(47)	0.2838(17)		
	0.17	0.26967(47)	0.2881(16)		
	0.18	0.27618(47)	0.2924(14)		
qP	0.12235(26)	0.26392(75)	0.2869(22)	0.3663(28)	0.235(22)
	0.11	0.25394(78)	0.2799(27)		
	0.12	0.26208(77)	0.2857(23)		
	0.13	0.26994(76)	0.2911(20)		
qW	0.07798(19)	0.25790(97)	0.2838(37)	0.3393(34)	0.216(24)
	0.07	0.2494(11)	0.2779(40)		
	0.08	0.2607(11)	0.2857(35)		
	0.09	0.2715(11)	0.2933(30)		
qX	0.05771(13)	0.25735(66)	0.2819(12)	0.3336(20)	0.2110(73)
	0.056	0.25480(69)	0.2801(13)		
	0.058	0.25780(68)	0.2822(12)		
	0.06	0.26073(68)	0.2842(12)		

Appendix A: Table of decay constants

All the results obtained on our ensembles are listed in Table 7.

Appendix B: Mass dependence of fermionic observables

Equation (4.36) describes how quantities with an explicit valence quark mass dependence depend on the quark mass, if decoupling is in place. The parameters of the leading order effective theory, here $N_f = 0$ QCD, are fixed by demanding non-perturbatively

$$\sqrt{t_0^{(2)}} = \sqrt{t_0^{(0)}}, \tag{B.1}$$

$$\sqrt{t_0^{(2)}}m_P^{(2)} = \sqrt{t_0^{(0)}}m_P^{(0)}. \tag{B.2}$$

The first condition fixes the scale

$$\Lambda^{(0)} = P_{2,0}(M^{(2)}/\Lambda^{(2)})\,\Lambda^{(2)}, \tag{B.3}$$

where $P_{2,0}$ is a matching function that can also be computed perturbatively, and which is unique up to $O(M^{-2})$ power corrections [46]. The second condition fixes the valence quark mass $M^{(0)}$ in the quenched theory. With just two dimensionful parameters in the game, M and Λ, every quantity of mass dimension one can be factorized into

$$X^{(N_f)}(M^{(N_f)}, \Lambda^{(N_f)}) = f_X^{(N_f)}(M^{(N_f)}/\Lambda^{(N_f)}) \, \Lambda^{(N_f)}, \quad \text{(B.4)}$$

with some dimensionless function f_X. In the fundamental $N_f = 2$ theory, Λ is constant, in the effective theory it depends on $M^{(2)} \equiv M$ through the decoupling relation Eq. (B.3). Moreover, f_X is constant in the effective theory for all quantities that do not depend on the valence quark mass $M^{(0)}$, e.g. all gluonic observables. Using the pseudoscalar meson mass to fix the $N_f = 0$ valence quark mass means that it is given by

$$M^{(0)} = f_{m_P}^{(0)^{-1}} \left(\frac{f_{m_P}^{(2)}(M/\Lambda^{(2)})}{P_{2,0}(M/\Lambda^{(2)})} \right) P_{2,0}(M/\Lambda^{(2)}) \, \Lambda^{(2)}. \text{(B.5)}$$

With this we can now evaluate

$$\eta_X^{(0)} = \frac{M}{X^{(0)}} \frac{dX^{(0)}}{dM} \tag{B.6}$$

$$= \frac{M}{X^{(0)}} \frac{df_X^{(0)}(M^{(0)}/\Lambda^{(0)})\Lambda^{(0)}}{dM}. \tag{B.7}$$

Both $\Lambda^{(0)}$ and $M^{(0)}$ depend on M, as outlined above. Inserting this dependence into the equation and carrying out the derivatives using the usual rules for derivatives of inverse functions, one finds

$$\eta_X^{(0)} = \eta^M + \frac{\tilde{\eta}_X^{(0)}}{\tilde{\eta}_{m_P}^{(0)}} \left(\eta_{m_P}^{(2)} - \eta^M \right) + O(M^{-2}), \tag{B.8}$$

where $\tilde{\eta}_X^{(0)} = \frac{M^{(0)}}{X} \frac{dX}{dM^{(0)}} \Big|_{\Lambda=\text{const}}$. The latter captures the valence quark mass dependence, but ignores the mass dependence of the scale in the effective theory.

References

1. S. Godfrey, S.L. Olsen, The exotic XYZ charmonium-like mesons. Ann. Rev. Nucl. Part. Sci. **58**, 51 (2008). https://doi.org/10.1146/annurev.nucl.58.110707.171145. arXiv:0801.3867

2. CDF collaboration, T. Aaltonen et al., Observation of the decay $B_c^\pm \to J/\psi \pi^\pm$ and measurement of the $B_c^\pm$ mass. Phys. Rev. Lett. **100**, 182002 (2008). https://doi.org/10.1103/PhysRevLett.100.182002. arXiv:0712.1506

3. D0 collaboration, V. Abazov et al., Observation of the B_c meson in the exclusive decay $B_c \to J/\psi \pi$. Phys. Rev. Lett. **101**, 012001 (2008). https://doi.org/10.1103/PhysRevLett.101.012001. arXiv:0802.4258]

4. Hadron Spectrum collaboration, L. Liu, G. Moir, M. Peardon, S.M. Ryan, C.E. Thomas, P. Vilaseca et al., Excited and exotic charmonium spectroscopy from lattice QCD. JHEP **07**, 126 (2012). https://doi.org/10.1007/JHEP07(2012)126. arXiv:1204.5425

5. Hadron Spectrum collaboration, G.K. Cheung, C. O'Hara, G. Moir, M. Peardon, S.M. Ryan, C.E. Thomas et al., Excited and exotic charmonium, D_s and D meson spectra for two light quark masses from lattice QCD. JHEP **12**, 089 (2016). https://doi.org/10.1007/JHEP12(2016)089. arXiv:1610.01073

6. Fermilab Lattice, MILC collaboration, C. DeTar, A.S. Kronfeld, S.h. Lee, D. Mohler, J.N. Simone, Splittings of low-lying charmonium masses at the physical point. Phys. Rev. D **99**, 034509 (2019). https://doi.org/10.1103/PhysRevD.99.034509. arXiv:1810.09983

7. F. Knechtli, Charmonium and exotics from lattice QCD. EPJ Web Conf. **202**, 01006 (2019). https://doi.org/10.1051/epjconf/201920201006. arXiv:1902.07079

8. HPQCD collaboration, D. Hatton, C. Davies, B. Galloway, J. Koponen, G. Lepage, A. Lytle, Charmonium properties from lattice QCD + QED: hyperfine splitting, J/ψ leptonic width, charm quark mass and a_μ^c. Phys. Rev. D **102**, 054511 (2020). https://doi.org/10.1103/PhysRevD.102.054511. arXiv:2005.01845

9. C. McNeile, C. Davies, E. Follana, K. Hornbostel, G. Lepage, Heavy meson masses and decay constants from relativistic heavy quarks in full lattice QCD. Phys. Rev. D **86**, 074503 (2012). https://doi.org/10.1103/PhysRevD.86.074503. arXiv:1207.0994

10. T. Korzec, F. Knechtli, S. Calì, B. Leder, G. Moir, Impact of dynamical charm quarks. PoS **LATTICE2016**, 126 (2017). https://doi.org/10.22323/1.256.0126. arXiv:1612.07634

11. S. Calì, F. Knechtli, T. Korzec, Comparison between models of QCD with and without dynamical charm quarks. PoS **LATTICE2018**, 082 (2018). https://doi.org/10.22323/1.334.0082. arXiv:1811.05285

12. ALPHA collaboration, S. Calì, F. Knechtli, T. Korzec, How much do charm sea quarks affect the charmonium spectrum?. Eur. Phys. J. C **79**, 607 (2019). https://doi.org/10.1140/epjc/s10052-019-7108-6. arXiv:1905.12971

13. J. Gasser, G. Zarnauskas, On the pion decay constant. Phys. Lett. B **693**, 122 (2010). https://doi.org/10.1016/j.physletb.2010.08.021. arXiv:1008.3479

14. C.T.H. Davies, C. McNeile, E. Follana, G.P. Lepage, H. Na, J. Shigemitsu, Update: precision D_s decay constant from full lattice QCD using very fine lattices. Phys. Rev. D **82**, 114504 (2010). https://doi.org/10.1103/PhysRevD.82.114504. arXiv:1008.4018

15. B. Blossier, J. Heitger, M. Post, leptonic D_s decays in two-flavour lattice QCD. Phys. Rev. D **98**, 054506 (2018). https://doi.org/10.1103/PhysRevD.98.054506. arXiv:1803.03065

16. F. Close, An Introduction to Quarks and Partons (1979)

17. S. Weinberg, Effective gauge theories. Phys. Lett. B **91**, 51 (1980). https://doi.org/10.1016/0370-2693(80)90660-7

18. W. Bernreuther, W. Wetzel, Decoupling of heavy quarks in the minimal subtraction scheme. Nucl. Phys. B **197**, 228 (1982). https://doi.org/10.1016/0550-3213(82)90288-7

19. K. Chetyrkin, J.H. Kühn, C. Sturm, QCD decoupling at four loops. Nucl. Phys. B **744**, 121 (2006). https://doi.org/10.1016/j.nuclphysb.2006.03.020. arXiv:hep-ph/0512060

20. Y. Schröder, M. Steinhauser, Four-loop decoupling relations for the strong coupling. JHEP **01**, 051 (2006). https://doi.org/10.1088/1126-6708/2006/01/051. arXiv:hep-ph/0512058

21. ALPHA collaboration, A. Athenodorou, J. Finkenrath, F. Knechtli, T. Korzec, B. Leder, M. Krstić Marinković et al., How perturbative are heavy sea quarks? Nucl. Phys. B **943**, 114612 (2019). https://doi.org/10.1016/j.nuclphysb.2019.114612. arXiv:1809.03383

22. ALPHA collaboration, F. Knechtli, T. Korzec, B. Leder, G. Moir, Power corrections from decoupling of the charm quark. Phys. Lett. B **774**, 649 (2017). https://doi.org/10.1016/j.physletb.2017.10.025. arXiv:1706.04982

23. ALPHA collaboration, R. Höllwieser, F. Knechtli, T. Korzec, Scale setting for $N_f = 3+1$ QCD. Eur. Phys. J. C **80**, 349 (2020). https://doi.org/10.1140/epjc/s10052-020-7889-7. arXiv:2002.02866

24. M. Lüscher, Properties and uses of the Wilson flow in lattice QCD. JHEP **08**, 071 (2010). https://doi.org/10.1007/JHEP08(2010)071. https://doi.org/10.1007/JHEP03(2014)092. arXiv:1006.4518

25. K.G. Wilson, Confinement of quarks. Phys. Rev. D **10**, 2445 (1974). https://doi.org/10.1103/PhysRevD.10.2445

26. B. Sheikholeslami, R. Wohlert, Improved continuum limit lattice action for QCD with Wilson fermions. Nucl. Phys. B **259**, 572 (1985). https://doi.org/10.1016/0550-3213(85)90002-1

27. ALPHA collaboration, R. Frezzotti, P.A. Grassi, S. Sint, P. Weisz, Lattice QCD with a chirally twisted mass term. JHEP **08**, 058 (2001). arXiv:hep-lat/0101001

28. R. Frezzotti, G. Rossi, Chirally improving Wilson fermions. 1. O(a) improvement. JHEP **08**, 007 (2004). https://doi.org/10.1088/1126-6708/2004/08/007. arXiv:hep-lat/0306014

29. M. Lüscher, S. Schaefer, Lattice QCD without topology barriers. JHEP **07**, 036 (2011). https://doi.org/10.1007/JHEP07(2011)036. arXiv:1105.4749

30. P. Fritzsch, F. Knechtli, B. Leder, M. Marinkovic, S. Schaefer, R. Sommer et al., The strange quark mass and Lambda parameter of two flavor QCD. Nucl. Phys. B **865**, 397 (2012). https://doi.org/10.1016/j.nuclphysb.2012.07.026. arXiv:1205.5380

31. ALPHA collaboration, P. Fritzsch, N. Garron, J. Heitger, Non-perturbative tests of continuum HQET through small-volume two-flavour QCD. JHEP **01**, 093 (2016). https://doi.org/10.1007/JHEP01(2016)093. arXiv:1508.06938

32. M. Lüscher, S. Sint, R. Sommer, H. Wittig, Nonperturbative determination of the axial current normalization constant in O(a) improved lattice QCD. Nucl. Phys. B **491**, 344 (1997). https://doi.org/10.1016/S0550-3213(97)00087-4. arXiv:hep-lat/9611015

33. M. Della Morte, R. Hoffmann, F. Knechtli, R. Sommer, U. Wolff, Non-perturbative renormalization of the axial current with dynamical Wilson fermions. JHEP **07**, 007 (2005).https://doi.org/10.1088/1126-6708/2005/07/007. arXiv:hep-lat/0505026

34. M. Dalla Brida, T. Korzec, S. Sint, P. Vilaseca, High precision renormalization of the flavour non-singlet Noether currents in lattice QCD with Wilson quarks. Eur. Phys. J. C **79**, 23 (2019). https://doi.org/10.1140/epjc/s10052-018-6514-5. arXiv:1808.09236

35. A. Jüttner, Precision Lattice Computations in the Heavy Quark Sector, Ph.D. thesis, Humboldt-Universität zu Berlin, Mathematisch-Naturwissenschaftliche Fakultät I (2004). https://doi.org/10.18452/15142

36. XLF collaboration, K. Jansen, A. Shindler, C. Urbach, I. Wetzorke, Scaling test for Wilson twisted mass QCD. Phys. Lett. B **586**, 432 (2004). https://doi.org/10.1016/j.physletb.2004.01.030. arXiv:hep-lat/0312013

37. S. Calì, Model Study of Charm Loop Effects, Ph.D. thesis, Wuppertal U. (2019). https://doi.org/10.25926/n9mr-f664

38. M. Bruno, T. Korzec, S. Schaefer, Setting the scale for the CLS 2 + 1 flavor ensembles. Phys. Rev. D **95**, 074504 (2017). https://doi.org/10.1103/PhysRevD.95.074504. arXiv:1608.08900

39. M. Bruno, The energy scale of the 3-flavour Lambda parameter, Ph.D. thesis, Humboldt U., Berlin (2015). https://doi.org/10.18452/17516

40. T. Appelquist, J. Carazzone, Infrared singularities and massive fields. Phys. Rev. D **11**, 2856 (1975). https://doi.org/10.1103/PhysRevD.11.2856

41. J. Heitger, G.M. von Hippel, S. Schaefer, F. Virotta, Charm quark mass and D-meson decay constants from two-flavour lattice QCD. PoS **LATTICE2013**, 475 (2014). https://doi.org/10.22323/1.187.0475. arXiv:1312.7693

42. Particle Data Group collaboration, M. Tanabashi et al., Review of particle physics. Phys. Rev. D **98**, 030001 (2018). https://doi.org/10.1103/PhysRevD.98.030001

43. ALPHA collaboration, J. Heitger, F. Joswig, S. Kuberski, Determination of the charm quark mass in lattice QCD with 2 + 1 flavours on fine lattices. arXiv:2101.02694

44. ALPHA collaboration, M. Della Morte, R. Hoffmann, F. Knechtli, J. Rolf, R. Sommer, I. Wetzorke et al., Non-perturbative quark mass renormalization in two-flavor QCD. Nucl. Phys. B **729**, 117 (2005). https://doi.org/10.1016/j.nuclphysb.2005.09.028. arXiv:hep-lat/0507035

45. ALPHA collaboration, M. Della Morte, R. Frezzotti, J. Heitger, J. Rolf, R. Sommer and U. Wolff, Computation of the strong coupling in QCD with two dynamical flavors. Nucl. Phys. B

46. ALPHA collaboration, M. Bruno, J. Finkenrath, F. Knechtli, B. Leder, R. Sommer, Effects of heavy sea quarks at low energies. Phys. Rev. Lett. **114**, 102001 (2015). https://doi.org/10.1103/PhysRevLett.114.102001. arXiv:1410.8374

47. G.M. de Divitiis, R. Petronzio, N. Tantalo, Distance preconditioning for lattice Dirac operators. Phys. Lett. B **692**, 157 (2010). https://doi.org/10.1016/j.physletb.2010.07.031 . arXiv:1006.4028

48. S. Collins, K. Eckert, J. Heitger, S. Hofmann, W. Söldner, Charmed pseudoscalar decay constants on three-flavour CLS ensembles with open boundaries. PoS **LATTICE2016**, 368 (2017). https://doi.org/10.22323/1.256.0368. arXiv:1701.05502

49. M. Lüscher, Solution of the Dirac equation in lattice QCD using a domain decomposition method. Comput. Phys. Commun. **156**, 209 (2004). https://doi.org/10.1016/S0010-4655(03)00486-7. arXiv:hep-lat/0310048

50. T. van Ritbergen, J.A.M. Vermaseren, S.A. Larin, The four-loop β-function in quantum chromodynamics. Phys. Lett. B **400**, 379 (1997). https://doi.org/10.1016/S0370-2693(97)00370-5. arXiv:hep-ph/9701390

51. M. Czakon, The four-loop QCD β-function and anomalous dimensions. Nucl. Phys. B **710**, 485 (2005). https://doi.org/10.1016/j.nuclphysb.2005.01.012. arXiv:hep-ph/0411261

52. P.A. Baikov, K.G. Chetyrkin, J.H. Kühn, Five-loop running of the QCD coupling constant. Phys. Rev. Lett. **118**, 082002 (2017). https://doi.org/10.1103/PhysRevLett.118.082002. arXiv:1606.08659

53. T. Luthe, A. Maier, P. Marquard, Y. Schröder, Towards the five-loop β-function for a general gauge group. JHEP **07**, 127 (2016). https://doi.org/10.1007/JHEP07(2016)127. arXiv:1606.08662

54. F. Herzog, B. Ruijl, T. Ueda, J.A.M. Vermaseren, A. Vogt, The five-loop β-function of Yang-Mills theory with fermions. JHEP **02**, 090 (2017). https://doi.org/10.1007/JHEP02(2017)090. arXiv:1701.01404

55. M. Dalla Brida, A. Ramos, The gradient flow coupling at high-energy and the scale of SU(3) Yang–Mills theory. Eur. Phys. J. C **79**, 720 (2019). https://doi.org/10.1140/epjc/s10052-019-7228-z. arXiv:1905.05147

56. N. Isgur, M.B. Wise, Weak decays of heavy mesons in the static quark approximation. Phys. Lett. B **232**, 113 (1989). https://doi.org/10.1016/0370-2693(89)90566-2

57. N. Isgur, M.B. Wise, Weak transition form factors between heavy mesons. Phys. Lett. B **237**, 527 (1990). https://doi.org/10.1016/0370-2693(90)91219-2

58. R. Sommer, Introduction to non-perturbative heavy quark effective theory, in *Les Houches Summer School: Session 93: Modern Perspectives in Lattice QCD: Quantum Field Theory and High Performance Computing*, p. 517 (2010). arXiv:1008.0710

59. ALPHA collaboration, J. Heitger, A. Jüttner, R. Sommer, J. Wennekers, Non-perturbative tests of heavy quark effective theory. JHEP **11**, 048 (2004). https://doi.org/10.1088/1126-6708/2004/11/048. arXiv:hep-ph/0407227

60. M. Bruno et al., Simulation of QCD with $N_f = 2 + 1$ flavors of non-perturbatively improved Wilson fermions. JHEP **02**, 043 (2015). https://doi.org/10.1007/JHEP02(2015)043. arXiv:1411.3982

61. RQCD collaboration, G.S. Bali, E.E. Scholz, J. Simeth, W. Söldner, Lattice simulations with $N_f = 2 + 1$ improved Wilson fermions at a fixed strange quark mass. Phys. Rev. D **94**, 074501 (2016). https://doi.org/10.1103/PhysRevD.94.074501. arXiv:1606.09039

62. HPQCD, UKQCD, MILC, Fermilab Lattice collaboration, C. Davies et al., High precision lattice QCD confronts experiment. Phys. Rev. Lett. **92**, 022001 (2004). https://doi.org/10.1103/PhysRevLett.92.022001. arXiv:hep-lat/0304004